Theoretical Investigation of Molecular Properties of the First Excited State of the Phenoxyl Radical

Chi-Wen Cheng, Yuan-Pern Lee, and Henryk A. Witek*

Institute of Molecular Science and Department of Applied Chemistry, National Chiao Tung University, 30010 Hsinchu, Taiwan

A theoretical study of molecular, electronic, and vibrational properties of the first excited state of the phenoxyl radical, A $^2B_2$, is presented. The calculated molecular geometries, vertical and adiabatic excitation energies, and harmonic vibrational frequencies are compared with analogous results obtained for the ground state. The calculated excitation energies correspond well to experimental data. The harmonic vibrational frequencies of the A $^2B_2$ and the ground state are similar except for modes involving the vibrations of the CO bond.

Introduction

The phenoxyl radical (C_6H_5O) has been a subject of intensive experimental and theoretical investigations over a long period of time.[1–7] This situation can be primarily attributed to a very important role that this radical plays in combustion and biological processes.[8,9] A considerable amount of information has been collected on the vibrational,[5] ESR,[10] and electronic[7] properties of C_6H_5O. The ground state of C_6H_5O, denoted as X $^2B_1$, is a doublet with an unpaired electron localized almost entirely in the π orbitals of the benzene ring.[5,10] No experimental data is available for the molecular structure of the radical. Theoretical calculations[5,6,11–14] show that the molecule has the C_{2v} symmetry with approximately double CO bond and a ring structure intermediate between aromatic and quinoid.[5] Almost a complete set of the ground state vibrational frequencies has been determined experimentally[15] using resonance Raman experiments,[4,16–18] gas-phase UV photoelectron spectroscopy,[19] and matrix-isolation polarized FTIR spectroscopy.[6] Harmonic vibrational frequencies of the ground state were calculated by many authors.[5,6,11–13,20] The lowest optically active electronic state of C_6H_5O is B $^2A_2$; it is located at approximately 2.0 eV above the ground state. The computed oscillator strength for the X $^2B_1 \rightarrow$ B $^2A_2$ transition is very small, which is consistent with very weak signal in the UV/vis spectrum.[7,21] The optimized geometry for this state was given by Liu et al.[14] and harmonic vibrational frequencies, by Johnston et al.[21] Next excited states, C $^2B_1$ and D $^2A_2$, were observed at 3.1 and 4.2 eV, respectively.[7] Theoretical predictions suggest that D $^2A_2$ is overlapping with another unobserved electronic state of symmetry $^2B_1$, which can be explained by a very small calculated oscillator strength of the latter state. (Note that the states B $^2A_2$ and D $^2A_2$ were erroneously quoted as B $^2A_1$ and D $^2A_1$ in refs 7 and 15.[22]) The highest observed electronic state of the phenoxyl radical, E $^2B_1$, is located at approximately 6.0 eV. All these observed states correspond to $\pi–\pi^*$ electronic transitions.

In this paper we present a theoretical study of the lowest electronically excited state of the phenoxyl radical, A $^2B_2$, which is located at approximately 1.1 eV above the ground state.[7,15,19] Because the transition X $^2B_1 \rightarrow$ A $^2B_2$ is optically dipole-forbidden, little is known about this state. It was first detected in a gas-phase ultraviolet photoelectron spectroscopy experi-

ment[19] at 1.06 eV. Subsequently, it was observed at 1.10 eV in a polarized FTIR study[7] for C_6H_5O isolated in cryogenic argon matrices. Unfortunately, the signal intensity—originating most probably from vibronic coupling—was too small to allow for a successful characterization of the A $^2B_2$ state. The vertical excitation energy for the A $^2B_2$ state was determined theoretically by several authors.[7,11,14,21,23–26] The most accurate estimations (1.03 eV with UB3LYP/cc-pVTZ[7] and 1.11 eV with UPBE/6-31(2+,2+)G(d,p)[26]) are obtained with time-dependent density functional theory (TDDFT). The optimized geometry of the phenoxyl radical in the A $^2B_2$ state was presented by Liu et al. at the UMP2/6-31G* level of theory.[14]

We present here the following properties of the phenoxyl radical in the A $^2B_2$ state: vertical excitation energies, adiabatic excitation energies, optimized geometries, and harmonic vibrational frequencies. The results are obtained using wave function and density based quantum chemical techniques. Along with the vibrational frequencies for C_6H_5O, we also present analogous data obtained for the isotopically substituted isomer, C_6D_5O. Our main motivation for presenting these results is a perspective of accurate experimental determination of molecular and optical properties of the A $^2B_2$ state of the phenoxyl radical using the cavity ringdown absorption spectroscopy.[27,28] We hope to present such a study in the near future.

Computational Details

The molecular model of phenoxyl radical is shown in Figure 1. Following the previous ground state studies,[5,7] we orient the molecule in the yz plane with the CO bond located on the z-axis. For both studied electronic states, the assumed molecular symmetry point group is C_{2v}. This choice is confirmed later by the calculated harmonic vibrational frequencies. The orientation of the molecule as described above allows for identifying the C_{2v} symmetry operations as follows: the C_2 axis is the z-axis, the σ_v plane is the xz plane, and the σ_v' plane is the yz plane. The chosen orientation also allows for labeling the molecular σ orbitals using the a_1 and b_2 irreps, and the molecular π orbitals, using the a_2 and b_1 irreps. In the chosen reference frame, the symmetry of the ground state is described as a doublet B_1 and the symmetry of the first excited state, as a doublet B_2.

The presented energies, geometries, and vibrational frequencies have been calculated using correlated quantum chemical

Molecular Properties of the Phenoxyl Radical

J. Phys. Chem. A, Vol. 112, No. 12, 2008 **2649**
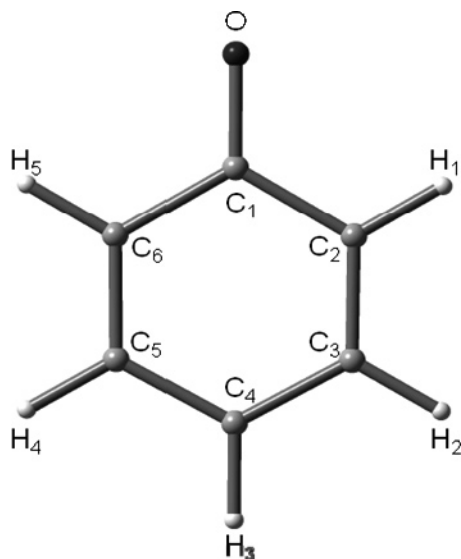

Figure 1. Molecular structure (C_{2v}) of the phenoxyl radical in the X $^2B_1$ and A $^2B_2$ electronic states.

techniques: the complete active space self-consistent field (CASSCF) method, complete active space second-order perturbation theory[29,30] (CASPT2), and density functional theory (DFT), and a set of four basis sets: cc-pVDZ, aug-cc-pVDZ, cc-pVTZ, and aug-cc-pVTZ.[31,32] For the multireference wavefunction-based calculations, we have used the MOLPRO program.[33] DFT and TDDFT calculations have been carried out using the Gaussian package.[34] In principle, DFT is a ground-state theory. However, it can also be formulated for excited states.[35] Gunnarsson and Lundqvist argued[36] that the validity of the Kohn−Sham scheme can be naturally extended to the energetically lowest electronic state in each of the symmetries with the same universal exchange-correlation functional. It was subsequently shown that this straightforward generalization works only if the electronic state in the non-interacting case reduces to a single Slater determinant.[37] Because, in many cases, the electronic nature of the excited states can be described well only by a multideterminantal wave function, it can be difficult to apply the technique of Gunnarsson and Lundqvist in a straightforward manner in a general case. Fortunately, the wave function of the first excited state of C_6H_5O is very well represented by a single Slater determinant and DFT can be applied for calculations on this state. We have found that the SCF optimization performed for the A $^2B_2$ state of the phenoxyl radical converged toward a local minimum in the orbital rotation space; i.e., all the unoccupied one-electron energy levels lie higher than all the occupied levels. The total energy of the global minimum in the orbital rotation space is approximately 1 eV lower; it corresponds to the ground state of the phenoxyl radical. All our DFT calculations, for both the ground and excited states, have used the same B3LYP functional[38,39] together with the unrestricted Kohn−Sham formalism.[40] We have also successfully used the Kohn−Sham ground state formalism to determine the vertical excitation energies for lowest excited states in each spatial or spin symmetry subspaces. The complete active space (CAS) in the CASSCF and CASPT2 calculations is constructed using all valence π orbitals (two of symmetry a_2 and five of symmetry b_1) and one or two orbitals corresponding to the lone pairs on the oxygen atom (one of symmetry a_1 and one of symmetry b_2). The two resultant active spaces, ($0a_1$, $2a_2$, $5b_1$, $1b_2$) and ($1a_1$, $2a_2$, $5b_1$, $1b_2$), correlate nine and eleven active electrons, respectively. The ($0a_1$, $2a_2$, $5b_1$, $1b_2$) active space has been used to optimize the geometry of both studied electronic

states of the phenoxyl radical, to calculate the vertical and adiabatic A $^2B_2 \leftarrow$ X $^2B_1$ excitation energies, and to determine harmonic vibrational frequencies. The larger active space, ($1a_1$, $2a_2$, $5b_1$, $1b_2$), has been used to determine the vertical excitation energies for the lowest doublet and quartet electronic states in each symmetry. The augmentation with an additional a_1 orbital has been necessary to describe properly the lowest $^2A_1$ and $^4A_1$ states of the phenoxyl radical.

Results

(a) Electronic and Geometrical Structure of the A $^2B_2$ State. The optimized CASPT2 and DFT geometrical parameters for the phenoxyl radical in the X $^2B_1$ and A $^2B_2$ electronic states are given in Table 1. We show the well-studied structure of the ground state together with the results obtained for the excited state A $^2B_2$ to facilitate the comparison of structural changes between these two states. The presented results constitute at the moment the most accurate theoretical estimations of the equilibrium structure for both studied states of C_6H_5O. A compilation of previously calculated equilibrium bond lengths and angles for the ground state is given in Supporting Information (Table S). The atom numbering used in the definition of geometrical parameters is shown in Figure 1. The two most prominent structural differences observed between the structures corresponding to these two electronic states are (i) increased length of the CO bond in the state A $^2B_2$ and (ii) different shape of the six-member carbon ring. For the ground state, the equilibrium distance between the carbon and oxygen atoms corresponds to a weak double CO bond. Compare the calculated values of 1.255 Å (CASPT2/aug-cc-pVTZ) and 1.252 Å (DFT/UB3LYP/aug-cc-pVTZ) with the experimental values of 1.215 Å for acetone, 1.205 Å for formaldehyde, 1.191 Å for cyclopropanone, 1.202 Å for cyclobutanone, 1.225 Å for p-benzoquinone, 1.216 Å for acetaldehyde, and 1.202 Å in acetic acid.[41,42] For the first excited state, the calculated length of the carbon-oxygen bond is similar to single CO bond. Compare the calculated values of 1.332 Å (CASPT2/aug-cc-pVTZ) and 1.321 Å (DFT/UB3LYP/aug-cc-pVTZ) with the experimental values of 1.364 Å for phenol, 1.377 Å for hydroquinone, 1.343 Å for formic acid, 1.361 Å for acetic acid, 1.362 Å for furan, 1.427 Å for methanol, 1.411 Å for dimethyl ether, 1.446 Å for oxetane, and 1.420 Å for ethanedial.[41,43] In the benzene molecule the equilibrium distance between the adjacent carbon atoms is equal to 1.397 Å.[41] Upon the substitution of one of the hydrogen atoms by some functional group, this regular pattern is somewhat perturbed. This perturbation has been usually neglected in the procedure of experimental determination of the equilibrium structure.[44] For example, the experimental equilibrium structures of phenol and aniline both assume a regular hexagon model for the benzene ring with average CC distance of 1.398 and 1.392 Å, respectively.[41,44] Recent experimental investigation[45] of the molecular structure of phenol shows that in fact the CC bond distances may differ noticeably (in the ground state the r_0 values are 1.383, 1.402, and 1.399, and in the S_1 state, they are 1.442, 1.452, and 1.422 Å). Similar information can be accessed directly from calculations. For phenol, the three unique CC bond lengths calculated using the DFT/B3LYP/6-31G(2df,p) computational scheme are 1.396, 1.393, and 1.392 Å, and for aniline, the analogous values are 1.402, 1.390, and 1.393 Å.[41] For phenoxyl radical in the ground state, this perturbation is much stronger. The calculated CASPT2/aug-cc-pVTZ equilibrium CC bond lengths are 1.448, 1.379, and 1.408 Å. The corresponding values obtained with DFT/UB3LYP/aug-cc-pVTZ are 1.448, 1.371, and 1.405 Å. This bond distance pattern is structurally

TABLE 1: Geometrical Parameters for the X $^2B_1$ and A $^2B_2$ States of the Phenoxyl Radical Optimized Using CASPT2 and DFT/B3LYP^a

	X $^2B_1$							
	cc-pVDZ		aug-cc-pVDZ		cc-pVTZ		aug-cc-pVTZ	
	CASPT2	B3LYP	CASPT2	B3LYP	CASPT2	B3LYP	CASPT2	B3LYP
r_{C_1O}	1.259	1.256	1.266	1.258	1.254	1.251	1.255	1.252
$r_{C_1C_2}$	1.461	1.455	1.461	1.455	1.448	1.449	1.448	1.448
$r_{C_2C_3}$	1.391	1.380	1.393	1.380	1.379	1.371	1.379	1.371
$r_{C_3C_4}$	1.420	1.412	1.421	1.412	1.408	1.405	1.408	1.405
$r_{C_2H_1}$	1.094	1.092	1.093	1.090	1.080	1.081	1.081	1.081
$r_{C_3H_2}$	1.094	1.093	1.093	1.091	1.081	1.082	1.081	1.082
$r_{C_4H_3}$	1.094	1.092	1.093	1.090	1.080	1.082	1.081	1.081
$\alpha_{C_6C_1C_2}$	117.1	117.0	117.6	117.3	117.3	117.0	117.5	117.1
$\alpha_{C_1C_2C_3}$	121.0	121.0	120.6	120.8	120.8	120.9	120.7	120.8
$\alpha_{C_2C_3C_4}$	120.2	120.2	120.3	120.3	120.2	120.3	120.3	120.3
$\alpha_{C_1C_2H_1}$	117.0	116.9	117.2	117.2	117.1	117.0	117.1	117.1
$\alpha_{C_4C_3H_2}$	119.6	119.5	119.6	119.5	119.6	119.4	119.6	119.4

	A $^2B_2$							
	cc-pVDZ		aug-cc-pVDZ		cc-pVTZ		aug-cc-pVTZ	
	CASPT2	B3LYP	CASPT2	B3LYP	CASPT2	B3LYP	CASPT2	B3LYP
r_{C_1O}	1.335	1.323	1.345	1.323	1.330	1.320	1.332	1.321
$r_{C_1C_2}$	1.415	1.413	1.415	1.413	1.402	1.405	1.402	1.405
$r_{C_2C_3}$	1.405	1.394	1.407	1.394	1.393	1.387	1.394	1.387
$r_{C_3C_4}$	1.407	1.397	1.408	1.397	1.394	1.389	1.395	1.389
$r_{C_2H_1}$	1.093	1.090	1.092	1.090	1.079	1.080	1.080	1.079
$r_{C_3H_2}$	1.094	1.093	1.093	1.093	1.081	1.082	1.081	1.082
$r_{C_4H_3}$	1.093	1.091	1.092	1.091	1.079	1.080	1.080	1.080
$\alpha_{C_6C_1C_2}$	120.6	119.9	121.2	119.9	120.9	120.1	121.1	120.1
$\alpha_{C_1C_2C_3}$	119.0	119.2	118.6	119.2	118.9	119.1	118.8	119.1
$\alpha_{C_2C_3C_4}$	121.1	121.4	121.1	121.4	121.1	121.4	121.1	121.4
$\alpha_{C_1C_2H_1}$	119.5	119.1	119.8	119.1	119.7	119.3	119.7	119.3
$\alpha_{C_4C_3H_2}$	120.2	120.2	120.1	120.2	120.2	120.1	120.1	120.1

^{a} All CASPT2 calculations use the same $(0a_1, 2a_2, 5b_1, 1b_2)$ active space described in detail in the text. Distances are given in Å and bonds, in degrees. For an explanation of geometrical parameters, see Figure 1.

similar to that one observed experimentally[42] for *p*-benzoquinone (1.477, 1.322, and 1.477 Å), which can be associated with an alternating chain of a single-double-single CC bonds. Chipman et al. described[5] the heavy-atom skeleton of the phenoxyl radical in the ground state as intermediate between aromatic and quinoid. In contrast with the ground state, the structure of the carbon ring in the first excited state, A $^2B_2$, is regular with similar length of all carbon—carbon bonds (1.402, 1.394, and 1.395 Å using CASPT2/aug-cc-pVTZ and 1.405, 1.387, and 1.389 Å using DFT/UB3LYP/aug-cc-pVTZ). Similarly, the calculated CCC angles are much closer to 120° than for the ground state. The structure of the carbon ring can then be described as almost aromatic with little quinoid character. Similar conclusion can be drawn from the previously published UMP2 results; however, this study[14] seems to underestimate the length of the CO bond in the ground state and overestimate it in the A $^2B_2$ state. The difference between the geometrical structures of the phenoxyl radical in the ground and the first excited states may be compared to the difference between the experimental structures of *p*-benzoquinone and hydroquinone.[42,43] The more aromatic character of the benzene ring in the A $^2B_2$ state can be anticipated from the π orbitals energy diagram shown in Figure 2. The energy pattern of the π orbitals in the A $^2B_2$ state is similar to that in benzene, whereas for the X $^2B_2$ state, the discrepancy is much larger. Moreover, for A $^2B_2$, the p_x orbital of oxygen strongly dominates the lowest π orbital of the b_1 symmetry and has only small contribution to other orbitals, whereas for X $^2B_2$, it contributes significantly to almost all π orbitals of the b_1 symmetry.

The electronic structure of the ground state and the first excited state of the phenoxyl radical and the corresponding transition between these two states can be described adequately within the framework of molecular orbital theory. We want to stress here that this is an unusual situation because in most cases the electronic structure of radicals—especially in excited electronic states—requires a multireference description. Before defining the Slater determinants corresponding to both wave functions, we describe chemically important molecular orbitals (MOs). We consider as such seven π orbitals, two MOs of symmetry a_2 and five MOs of symmetry b_1, and two σ orbitals, being the a_1 and b_2 linear combinations of the lone electron pairs on the oxygen atom. The remaining occupied σ molecular orbitals—twelve of symmetry a_1 and seven of symmetry b_2—have considerably lower energy, and they remain doubly occupied in all important Slater determinants. To define the chemical character of the seven lowest π orbitals we compare their one-electron energies with the weighted average of the ϵ_{2p} energies of carbon and oxygen (dotted horizontal line in Figure 2). The actual value of such an average obtained from atomic calculations is approximately equal to −0.10 hartree for all employed basis sets. Therefore, MOs with $\epsilon < -0.10$ are classified as bonding (π) and MOs with $\epsilon > -0.10$, as antibonding (π^*). The orbitals with $\epsilon \approx -0.10$ are referred to as nonbonding (π°). One-electron energy diagrams of the π orbitals for both electronic states of C_6H_5O are shown in Figure 2. A schematic representation of the π orbitals as the linear combinations of the atomic p_x orbitals is given in Figure 3. For the ground state, the three lowest π orbitals, two of symmetry b_1 and one of symmetry a_2, are strongly bonding whereas the singly occupied b_1 orbital is nonbonding. For the first excited state, the four lowest π orbitals, three of symmetry b_1 and one
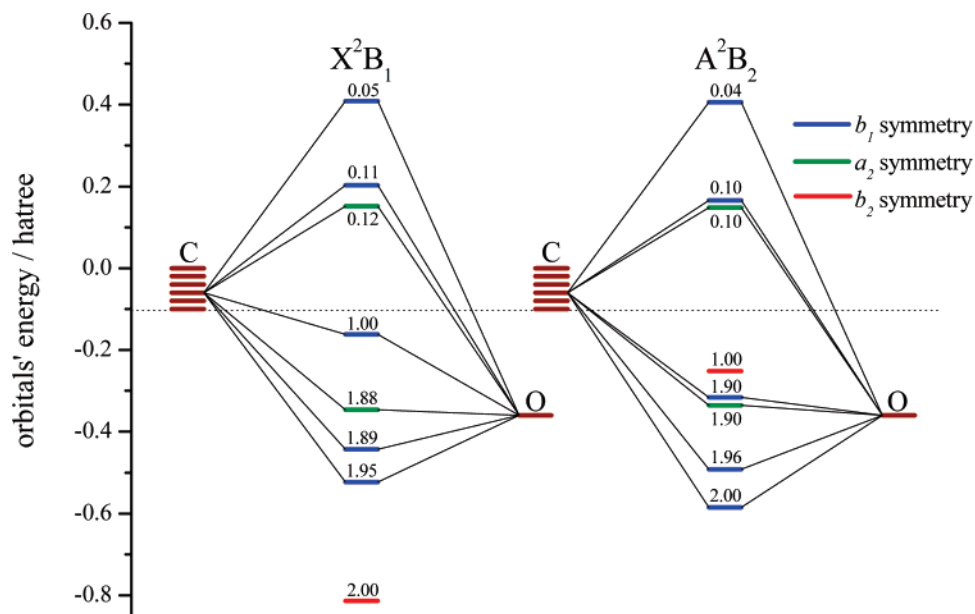
Molecular Properties of the Phenoxyl Radical

J. Phys. Chem. A, Vol. 112, No. 12, 2008 **2651**

Figure 2. Orbital energy diagram for the seven active π orbitals and one active σ orbital of C_6H_5O in the X $^2B_1$ and A $^2B_2$ states obtained from the CASSCF($0a_1$, $2a_2$, $5b_1$, $1b_2$)/aug-cc-pVDZ calculations. Occupation numbers are given for every orbital.
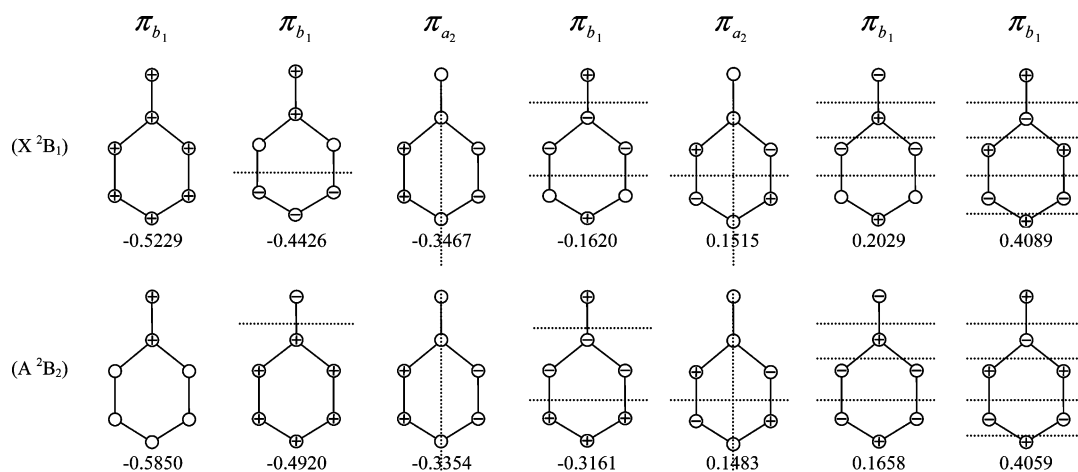

Figure 3. Schematic representation of the seven active π orbitals in the X $^2B_1$ and A $^2B_2$ states of C_6H_5O. Nodal planes are given by dotted lines. The symbol in each circle denotes the sign of the linear combination coefficient for the p_x orbitals at the CASSCF($0a_1$, $2a_2$, $5b_1$, $1b_2$)/aug-cc-pVDZ level. The empty circle represents a coefficient value close to zero. Orbital energies are given in hartree.

of symmetry a_2, are strongly bonding. The remaining π orbitals are classified as antibonding.

In the ground state of the phenoxyl radical the dominant Slater determinant can be defined as $|\sigma_{a_1}^2 \pi_{b_1}^2 \sigma_{b_2}^2 \pi_{b_1}^2 \pi_{a_2}^2 \pi_{b_1}^{o1} \pi_{a_2}^{*0} \pi_{b_1}^{*0} \pi_{b_1}^{*0}\rangle$, with a singly occupied π orbital being a linear combination of the p_x orbitals on oxygen and the π orbitals of the benzene ring (see Figure 3). The percentage contribution of this configuration in the CASSCF wave function is 83%. The next three most important configurations, $|\sigma_{a_1}^2 \pi_{b_1}^2 \sigma_{b_2}^2 \pi_{b_1}^1 \pi_{a_2}^2 \pi_{b_1}^{o1} \pi_{a_2}^{*0} \pi_{b_1}^{*1} \pi_{b_1}^{*0}\rangle$, $|\sigma_{a_1}^2 \pi_{b_1}^2 \sigma_{b_2}^2 \pi_{b_1}^2 \pi_{a_2}^1 \pi_{b_1}^{o1} \pi_{a_2}^{*1} \pi_{b_1}^{*0} \pi_{b_1}^{*0}\rangle$, and $|\sigma_{a_1}^2 \pi_{b_1}^2 \sigma_{b_2}^2 \pi_{b_1}^2 \pi_{a_2}^2 \pi_{b_1}^{o1} \pi_{a_2}^{*2} \pi_{b_1}^{*0} \pi_{b_1}^{*0}\rangle$, correspond to various distribution of electrons in the aromatic π orbitals with the percentage contribution to the CASSCF wave function of 2.9%, 2.2%, and 2.0%, respectively. After accounting for dynamical correlation, the contribution of these leading configurations to the CASPT2 wave function is 64%, 2.2%, 1.7%, and 1.5%, respectively. For the first excited state, A $^2B_2$, the leading electronic configuration, $|\pi_{b_1}^2 \sigma_{a_1}^2 \pi_{b_1}^2 \pi_{a_2}^2 \pi_{b_1}^2 \sigma_{b_2}^1 \pi_{a_2}^{*0} \pi_{b_1}^{*0} \pi_{b_1}^{*0}\rangle$, contributes 88% to the CASSCF wave function. The analogous contributions from the next three Slater determinants,

$|\pi_{b_1}^2 \sigma_{a_1}^2 \pi_{b_1}^2 \pi_{a_2}^0 \pi_{b_1}^2 \sigma_{b_2}^1 \pi_{a_2}^{*2} \pi_{b_1}^{*0} \pi_{b_1}^{*0}\rangle$, $|\pi_{b_1}^2 \sigma_{a_1}^2 \pi_{b_1}^2 \pi_{a_2}^2 \pi_{b_1}^0 \sigma_{b_2}^1 \pi_{a_2}^{*0} \pi_{b_1}^{*2} \pi_{b_1}^{*0}\rangle$, and $|\pi_{b_1}^2 \sigma_{a_1}^2 \pi_{b_1}^1 \pi_{a_2}^2 \pi_{b_1}^1 \sigma_{b_2}^1 \pi_{a_2}^{*1} \pi_{b_1}^{*1} \pi_{b_1}^{*1}\rangle$ are 2.2%, 2.2%, and 2.0%, respectively. After accounting for dynamical correlation, the contribution from these leading configurations reduces to 68%, 1.7%, 1.7%, and 1.5%. The presented numerical results have been derived with the cc-pVDZ basis set. For larger basis sets, the calculated contributions to the CASSCF wave functions have similar values, whereas the contributions to the CASPT2 wave functions undergo further reductions owing to a larger portion of dynamical correlation covered by these basis sets. To complete the discussion of the character of wave functions for both electronic states, we have to add that that the occupation numbers for the antibonding active π orbitals are non-negligible: 0.12, 0.11, and 0.05 for the ground state and 0.10, 0.10, and 0.04 for the A $^2B_2$ state, which suggest considerable static correlation in the aromatic ring despite a single-determinant character of both wave functions.

According to the above discussion, the A $^2B_2$ ← X $^2B_1$ excitation can be described as a transfer of a single electron
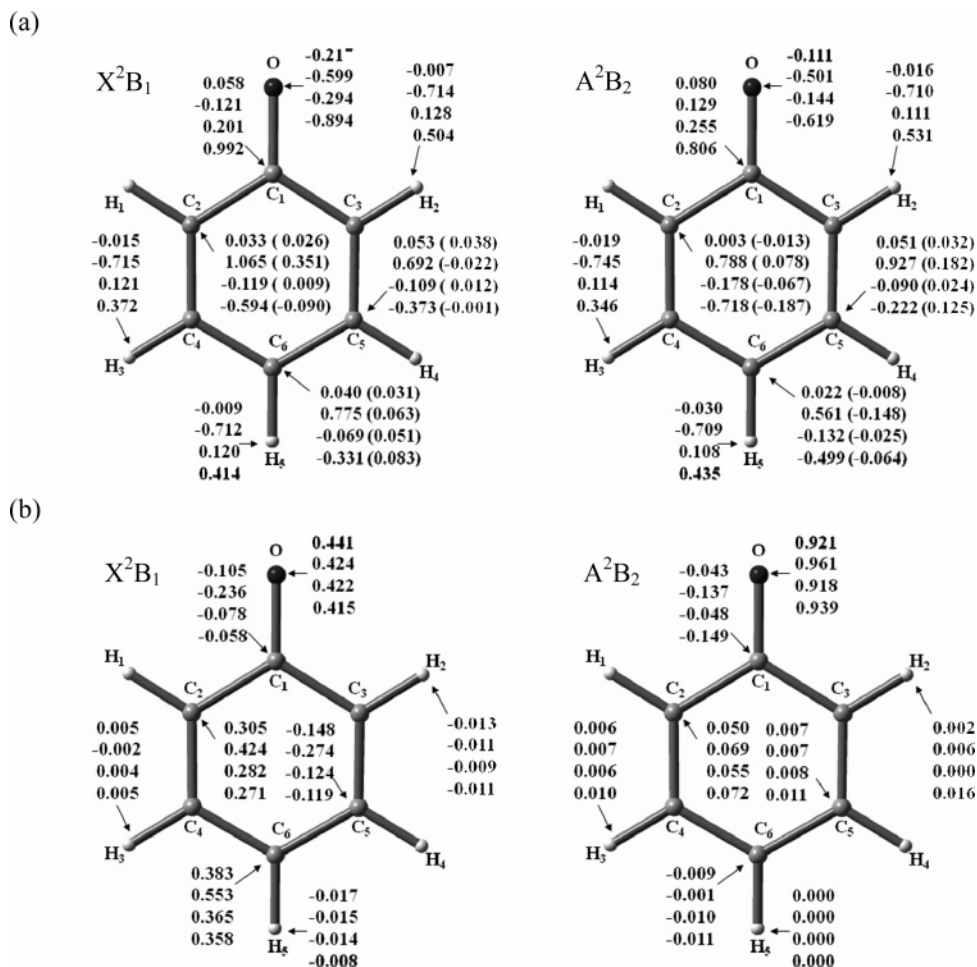
Figure 4. Mulliken charges (a) and spin densities (b) for the X $^2B_1$ and A $^2B_2$ states of C_6H_5O obtained from DFT calculation in four basis set (cc-pVDZ, aug-cc-pvDZ, cc-pVTZ, aug-cc-pVTZ). Values in parentheses correspond to induced atomic charges with hydrogen contributions summed into adjacent carbon atoms.

TABLE 2: Total Energies, Vertical Excitation Energies, and Adiabatic Excitation Energies for the X $^2B_1$ and A $^2B_2$ Electronic States of Phenoxyl Radical Computed Using the CASPT2 and DFT/B3LYP Methods[a]

	total energies			A $^2B_2$←X $^2B_1$ excitation energies			
basis set	X $^2B_1$	A $^2B_2$ (vertical)	A $^2B_2$ (adiabatic)	vertical[b]	adiabatic	ΔE_H^{0-0}	ΔE_D^{0-0}
			CASPT2				
cc-pVDZ	−305.920944	−305.876788	−305.884349	1.202	0.996	0.995	0.993
aug-cc-pVDZ	−305.972746	−305.926807	−305.934095	1.250	1.052	1.049	1.047
cc-pVTZ	−306.210241	−306.165644	−306.173021	1.214	1.013	1.010	1.008
aug-cc-pVTZ	−306.231793	−306.186453	−306.193693	1.234	1.037	1.034	1.032
			B3LYP				
cc-pVDZ	−306.847702	−306.810021	−306.815859	1.025 (0.983)	0.867	0.865	0.864
aug-cc-pVDZ	−306.866905	−306.827708	−306.833555	1.067 (1.035)	0.908	0.904	0.903
cc-pVTZ	−306.939129	−306.900562	−306.906565	1.050 (1.029)	0.886	0.883	0.881
aug-cc-pVTZ	−306.943226	−306.904275	−306.910234	1.060 (1.045)	0.898	0.895	0.893
exp				1.06[c], 1.10[d]			

[a] All CASPT2 calculations use the same $(0a_1, 2a_2, 5b_1, 1b_2)$ active space described in detail in the text. ΔE_H^{0-0} denotes the 0−0 excitation energy for C_6H_5O and ΔE_D^{0-0}, for C_6D_5O. Total energies are given in hartree and excitation energies, in eV. [b] Values in parentheses have been calculated using the TDDFT method. [c] Reference 19, in the gas phase. [d] Reference 7, in an argon matrix.

from the lone pair (or more precisely: the b_2 linear combination of the lone pairs on oxygen) on the oxygen atom to the nonbonding $\pi_{b_1}^o$ orbital delocalized over the oxygen atom and the aromatic ring. This transfer causes a considerable stabilization of the π orbitals system and results in a substantial lowering of the $\pi_{b_1}^o$ orbital energy and a significant raise of the one-electron energy of the singly occupied σ_{b_2} orbital. Note that these findings contradict the usual classification of the A $^2B_2$ ← X $^2B_1$ excitation as the $n-\pi^*$ transition. The correct

assignment should read $n-\pi^o$ or even $n-\pi$, if one takes into account the substantial stabilization of the resultant doubly occupied π_{b1} orbital. The Mulliken charges extracted from the DFT/UB3LYP/cc-pVDZ calculations show that for the ground state, a fractional negative charge of 0.22 is located on the oxygen atom, whereas the corresponding positive charge is distributed almost equally over all carbon atoms. For the first excited state, the induced negative charge on the oxygen atom is smaller (0.11) and the corresponding positive charge is located

Molecular Properties of the Phenoxyl Radical

J. Phys. Chem. A, Vol. 112, No. 12, 2008 **2653**

primarily on the adjacent and the *meta* carbon atoms. The Mulliken charges extracted from the DFT calculations in larger basis sets confirm this trend, but at the same time show very strong dependence on the size of the basis set. (For details, see Figure 4.) This dependence is somewhat diminished by including the induced charge on hydrogens into the neighboring carbons but still does not provide a sound basis for further analysis. Figure 4 shows that the calculated spin densities are more reliable source of information about the actual charge distribution in the phenoxyl radical molecule. The analysis of the cc-pVDZ DFT spin densities shows that for the ground state, the single electron is strongly delocalized over the oxygen atom (0.44) and the aromatic ring (−0.10, +0.30, −0.15, and +0.38 for the adjacent, *ortho*, *meta*, and *para* carbon atoms, respectively), but for the A $^2B_2$ state, it is almost entirely localized on the oxygen atom (0.92). This situation is in contrast with that in the recently studied[46,47] phenylthiyl radical (C_6H_5S), where the single electron was strongly localized on the sulfur atom in both electronic states. The shape of the singly occupied molecular orbital (SOMO) in both electronic states coincided with the atomic-like p_x or p_y orbitals of sulfur. The large degree of localization and the similarity of SOMO to the atomic orbitals of sulfur motivated the authors to use the term "intramolecular orbital alignment" while discussing the orientation of the SOMO orbital with respect to the molecular frame of reference. Our study shows that for C_6H_5O, the out-of-plane SOMO orbital is strongly delocalized over the whole aromatic ring. We believe that the main reason for this large degree of delocalization is much shorter distance between carbon and oxygen (1.252 Å using DFT/UB3LYP/aug-cc-pVTZ) than between carbon and sulfur (1.723 Å using DFT/UB3LYP/aug-cc-pVTZ) leading to more effective mixing of the p_x orbitals of oxygen and carbon in C_6H_5O than the p_x orbitals of sulfur and carbon in C_6H_5S. Therefore, the "intramolecular orbital alignment" phenomenon,[46,47] observed for C_6H_5S, is not confirmed for C_6H_5O by our theoretical calculations.

The comparison of the equilibrium geometry of both studied electronic states with their electronic structures gives somewhat counterintuitive conclusions. One may expect that transferring an electron from the nonbonding electron pair on the oxygen atom to the system of π orbitals may result in strengthening the π bond system, which is ensued by shortening the CO bond. However, the optimized geometrical parameters show that the bond in fact becomes longer and loses its approximate double character. This rather surprising observation can be qualitatively understood by studying the composition of the bonding π orbitals given in Figure 3. Note that for discussing the bond order between carbon and oxygen, only the b_1 orbitals are relevant, because the nodal structure of the a_2 orbitals enforces zero contribution from the p_x orbitals on oxygen and on the adjacent carbon atom. For the ground state of the phenoxyl radical, the two lowest b_1 orbitals contribute to the π bond between oxygen and carbon; this bond is slightly weakened by the antibonding contribution from the SOMO orbital, which has a nodal plane between the C and O atoms (see Figure 3). For the first excited state, the bonding contribution from the lowest b_1 orbital is almost entirely cancelled by the antibonding contributions from the next two b_1 orbitals, which have nodal planes located between oxygen and the adjacent carbon. This analysis explains then the approximate double character of the CO bond in the ground state and the approximate single character of this bond in the first excited state. Note that this situation is quantitatively different than that observed[46,47] for the phenylthiyl radical (C_6H_5S), where the bond distance

TABLE 3: Vertical Excitation Energies (in eV) for the Lowest Doublet and Quartet Excited States of the Phenoxyl Radical Computed Using the CASSCF, CASPT2, and DFT/B3LYP Methods[a]

	CASSCF				CASPT2				TDDFT[e] (DFT)				exp[e]
	cc-pVDZ	aug-cc-pVDZ	cc-pVTZ	aug-cc-pVTZ	cc-pVDZ	aug-cc-pVDZ	cc-pVTZ	aug-cc-pVTZ	cc-pVDZ	aug-cc-pVDZ	cc-pVTZ	aug-cc-pVTZ	
X$^2B_1$	−305.060620	−305.072141	−305.138148	−305.140843	−305.920967	−305.972759	−306.210162	−306.231701	−306.846951	−306.866236	−306.939128	−306.943223	0
A$^2B_2$	1.312	1.358	1.349	1.356	1.187	1.236	1.198	1.218	0.983 (1.025)	1.035 (1.067)	1.029 (1.050)	1.045 (1.060)	1.06, 1.10
B$^2A_2$	2.560	2.511	2.557	2.542	2.228	2.109	2.184	2.139	2.409 (2.429)	2.319 (2.332)	2.381 (2.395)	2.348 (2.361)	1.98, 2.03
C$^2B_1$	3.440	3.460	3.496	3.500	3.158	3.197[c]	3.122	3.228[c]	3.582 (...)	3.531 (...)	3.588 (...)	3.566 (...)	3.12
1$^4B_1$	4.231	4.220	4.293	4.289	4.200	4.166[b]	4.226	4.239[c]	... (4.375)	... (4.336)	... (4.421)	... (4.402)	
1$^4B_2$	4.857	4.847	4.904	4.888	4.742[b]	4.708[b]	4.731	4.852[c]	5.891[f] (5.583)	5.948[f] (5.572)	5.997[f] (5.651)	6.010[f] (5.636)	
1$^4A_2$	5.661	5.639	5.721	5.714	5.343	5.346[c]	5.337	5.401[c]	5.476[f] (5.593)	5.367[f] (5.451)	5.488[f] (5.581)	5.435[f] (5.511)	
1$^4A_1$	5.793	5.775	5.822	5.808	4.939	4.882[b]	4.893	4.893[b]	4.760[f] (4.847)	4.775[f] (4.814)	4.821[f] (4.864)	4.821[f] (4.841)	
1$^2A_1$	5.976	5.960	6.015	6.000	5.383[c]	5.432[d]	5.312[c]	5.432[d]	4.907 (4.916)	4.859 (4.865)	4.903 (4.901)	4.879 (4.876)	

[a] All the CASSCF/CASPT2 calculation use the same (1a₁, 2a₂, 5b₁, 1b₂) active space described in detail in the text. Lowest excited state in each symmetry is given. [b] Level shift α = 0.1 has been used to avoid intruder states. [c] Level shift α = 0.2 has been used to avoid intruder states. [d] Level shift α = 0.3 has been used to avoid intruder states. [e] Reference 15. [f]TDDFT values for 1⁴B₂, 1⁴A₂, and 1⁴A₁ are calculated using the 1⁴B₁ reference function.

TABLE 4: Harmonic Vibrational Frequencies (Scaled) for the A $^2B_2$ Electronic State of C_6H_5O Computed Using the DFT/B3LYP and CASSCF Methods[a]

symmetry	mode	CASSCF		B3LYP			
		cc-pVDZ	aug-cc-pVDZ	cc-pVDZ	aug-cc-pVDZ	cc-pVTZ	aug-cc-pVTZ
A_1	ν_1	3085	3083	3108	3107	3098	3100
	ν_2	3073	3070	3099	3098	3088	3091
	ν_3	3054	3054	3069	3070	3059	3062
	ν_4	1599	1591	1570	1556	1559	1556
	ν_5	1483	1476	1403	1393	1412	1410
	ν_6	1252	1233	1228	1201	1207	1202
	ν_7	1146	1147	1143	1143	1154	1152
	ν_8	999	999	1012	1008	1012	1011
	ν_9	973	968	955	953	961	961
	ν_{10}	794	789	802	797	803	802
	ν_{11}	508	501	502	501	506	505
A_2	ν_{12}	894	885	934	928	936	941
	ν_{13}	769	761	797	787	797	799
	ν_{14}	396	396	416	414	417	416
B_1	ν_{15}	916	899	950	943	948	955
	ν_{16}	824	813	855	847	857	861
	ν_{17}	698	690	710	697	708	710
	ν_{18}	650	634	675	674	676	673
	ν_{19}	479	469	501	490	498	496
	ν_{20}	230	230	223	218	221	219
B_2	ν_{21}	3080	3077	3107	3106	3097	3099
	ν_{22}	3063	3061	3074	3075	3064	3067
	ν_{23}	1567	1563	1539	1529	1531	1529
	ν_{24}	1429	1427	1406	1395	1410	1408
	ν_{25}	1303	1305	1297	1291	1306	1304
	ν_{26}	1190	1192	1235	1232	1222	1222
	ν_{27}	1085	1081	1128	1130	1141	1139
	ν_{28}	1047	1046	1053	1052	1058	1058
	ν_{29}	603	608	600	599	605	604
	ν_{30}	367	367	357	354	358	358

[a] For a description of the active space of CASSCF, see the text. All values are given in cm^{-1}.

between sulfur and the adjacent carbon is similar in both electronic states (1.723 Å for X $^2B_1$ and 1.763 Å for A $^2B_2$; DFT/UB3LYP/aug-cc-pVTZ calculations). Such a bond length is intermediate between typical aromatic ($r_{CS} = 1.714$ Å in thiophene[41]) and single bonds ($r_{CS} = 1.818$ Å in methanethiol[41]). It is noticeably longer than a characteristic double CS bond ($r_{CS} = 1.611$ Å in thioformaldehyde[41]). We believe that the necessity of breaking the π bond in phenoxyl radical upon the A $^2B_2 \leftarrow$ X $^2B_1$ excitation is responsible for significantly higher excitation energy—compare 0.37 eV for C_6H_5S vs 1.06 eV for C_6H_5O—required for this transition.

(b) Vertical and Adiabatic A $^2B_2 \leftarrow$ X $^2B_1$ Excitation Energies. The calculated values of vertical and adiabatic A $^2B_2 \leftarrow$ X $^2B_1$ excitation energies for the phenoxyl radical are given in Table 2. The presented values have been obtained using the CASPT2, DFT/UB3LYP, and TDDFT/UB3LYP methods.[48] The analogous results obtained with the CASSCF method are given in Table K of the Supporting Information; we do not present these values here because the CASSCF energetics is usually not very accurate. It is difficult to state clearly which method reproduces the experimental data best, because of not obvious character of the experimental findings. If one assumes that the experimental energies of 1.10 and 1.06 eV correspond to vertical excitation, then the DFT/UB3LYP and TDDFT/UB3LYP methods seem to reproduce the experimental data most accurately. If, on the contrary, one assumes that they correspond to adiabatic excitation, then the correspondence of the CASPT2 results to experiment is better. The difference between the calculated DFT and CASPT2 excitation energies is approximately constant; the later are consistently 0.13 eV higher for all employed basis sets. Such a discrepancy is considered to be within the error bar for typical second-order multireference perturbation theory calculations.[49–51] This discrepancy is some-

what smaller if the larger active space is used in the CASPT2 calculations. The CASPT2 vertical excitation energies shown in Table 3, which have been computed using the ($1a_1$, $2a_2$, $5b_1$, $1b_2$) active space, are approximately 0.015 eV smaller than those calculated with the ($0a_1$, $2a_2$, $5b_1$, $1b_2$) active space (Table 2). To compute quantities that can be directly compared to experiment, we have calculated the 0–0 transition energies between the A $^2B_2$ and X $^2B_1$ states of C_6H_5O and C_6D_5O. In fact, these values differ only slightly from the adiabatic excitation energies owing to almost identical zero-point energy corrections for both states. Note that we refer here to the adiabatic excitation energy as a difference between the minima of the calculated potential energy curves. The zero-point corrections have been calculated using the scaled harmonic vibrational frequencies computed separately for each basis set using the DFT/UB3LYP procedure (for details, see below). Because the CASPT2 frequencies could not be easily accessed, we have used the calculated DFT frequencies to estimate also the CASPT2 (Table 2) and CASSCF (Table K of Supporting Information) 0–0 transition energies.

Vertical excitation energies for low-lying doublet and quartet states of the phenoxyl radical are given in Table 3. The presented results are calculated using the CASSCF, CASPT2, DFT, and TDDFT methods. For the CASSCF and CASPT2 calculations, we have used the extended ($1a_1$, $2a_2$, $5b_1$, $1b_2$) active space. We have decided to include these results in the present paper to visualize the energetics of the low-lying quartet states that can be easily studied using the CASSCF and CASPT2 techniques. As expected, the calculated excitation energies for the lowest quartet states are rather large. The lowest quartet state is $^4B_1$ located at approximately 4.2 eV higher than the ground state. Determination of CASPT2 energies for many of the high-lying excited states of C_6H_5O required using large values of

Molecular Properties of the Phenoxyl Radical

J. Phys. Chem. A, Vol. 112, No. 12, 2008 **2655**

TABLE 5: Harmonic Vibrational Frequencies (Scaled) for the A $^2B_2$ Electronic State of C_6D_5O Computed Using the DFT/B3LYP and CASSCF Methods[a]

symmetry	mode	CASSCF		B3LYP			
		cc-pVDZ	aug-cc-pVDZ	cc-pVDZ	aug-cc-pVDZ	cc-pVTZ	aug-cc-pVTZ
A_1	ν_1	2298	2299	2311	2312	2307	2306
	ν_2	2283	2284	2300	2301	2296	2295
	ν_3	2262	2265	2268	2272	2266	2266
	ν_4	1565	1559	1538	1525	1525	1521
	ν_5	1382	1368	1286	1269	1278	1274
	ν_6	1186	1175	1200	1179	1188	1183
	ν_7	937	936	925	922	931	930
	ν_8	856	857	855	853	863	862
	ν_9	819	821	814	816	826	824
	ν_{10}	740	737	740	738	745	744
	ν_{11}	497	490	492	491	497	495
A_2	ν_{12}	721	715	760	758	764	768
	ν_{13}	600	594	622	615	623	624
	ν_{14}	352	351	364	361	366	364
B_1	ν_{15}	747	724	792	799	794	804
	ν_{16}	695	681	725	716	726	726
	ν_{17}	586	575	587	576	586	585
	ν_{18}	529	527	546	539	548	544
	ν_{19}	418	411	432	424	430	429
	ν_{20}	219	219	211	206	210	208
B_2	ν_{21}	2292	2292	2306	2307	2301	2301
	ν_{22}	2272	2274	2276	2279	2273	2273
	ν_{23}	1531	1528	1506	1498	1496	1493
	ν_{24}	1305	1301	1325	1314	1315	1312
	ν_{25}	1145	1140	1234	1228	1219	1218
	ν_{26}	1021	1025	998	996	1016	1014
	ν_{27}	828	829	818	820	831	829
	ν_{28}	802	804	798	801	811	809
	ν_{29}	581	586	576	576	583	581
	ν_{30}	355	355	345	343	347	346

[a] For a description of the active space of CASSCF, see the text. All values are given in cm^{-1}.

level shift to avoid intruder states, especially when using augmented basis sets. TDDFT yields more accurate excitation energies than CASSCF and CASPT2 for the lowest excited state, A $^2B_2$. (See the discussion above about the character of experimental excitation energies.) For the higher states, B $^2A_2$ and C $^2B_1$, the CASPT2 method seems to be the most accurate with an average error of 0.10−0.15 eV, whereas the error of CASSCF and TDDFT can be as large as 0.3−0.5 eV. It is interesting to mention here that by solving the ground-state Kohn−Sham equations in each symmetry and/or spin subspace we have been able to obtain DFT vertical excitation energies of similar (or even better) quality like from the corresponding TDDFT calculations.

(c) Harmonic Vibrational Frequencies. Harmonic vibrational frequencies for the A $^2B_2$ state of C_6H_5O calculated using the CASSCF and DFT/UB3LYP methods are given in Table 4. Analogous results computed for C_6D_5O are presented in Table 5. To analyze the change of vibrational frequencies upon the A $^2B_2 \leftarrow$ X $^2B_1$ excitation, we have calculated also the harmonic vibrational frequencies for the ground state of phenoxyl radical. These results are presented in the Supporting Information (Table X1 for C_6H_5O and Table X2 for C_6D_5O). Because both the CASSCF and DFT harmonic vibrational frequencies have large systematic errors, the computed frequencies have been scaled to ensure better correspondence to experiment. We have used a single scaling factor for all type of vibrations. The scaling factors for each basis set and for each employed method have been computed separately using as a reference the well-known experimental frequencies of phenol.[52,53] The calculated CASSCF and DFT frequencies of phenol together with the determined scaling factors are presented in Supporting Information (Tables P1, P2, P3, and P4). The scaling factors for a given method vary only slightly upon the change of basis set or isotope

substitution. For the DFT/B3LYP procedure, the computed scaling factors are 0.967 for cc-pVDZ, 0.967 for aug-cc-pVDZ, 0.966 for cc-pVTZ, and 0.967 for aug-cc-pVTZ for the C_6H_5OH molecule and 0.970 for cc-pVDZ, 0.971 for aug-cc-pVDZ, 0.971 for cc-pVTZ, and 0.971 for aug-cc-pVTZ for the C_6D_5OD molecule. For the CASSCF procedure, the analogous factors are 0.915 (cc-pVDZ) and 0.917 (aug-cc-pVDZ) for C_6H_5OH and 0.919 (cc-pVDZ) and 0.922 (aug-cc-pVDZ) for C_6D_5OD. It would be very valuable to obtain some computational error estimates for the calculated vibrational frequencies of C_6H_5O and C_6D_5O in the A $^2B_2$ state. To this end, we have compared the calculated scaled harmonic vibrational frequencies for the ground states of C_6H_5OH, C_6D_5OD, C_6H_5O, and C_6D_5O with the corresponding experimental data. The standard deviations and maximal absolute deviations obtained with different computational procedures are presented in Table 6. The deviations for the CASSCF method are considerably larger than those calculated using the DFT data. The smallest deviations are obtained for the DFT/B3LYP method and the cc-pVTZ basis set. For the rest of this section, we analyze the vibrational spectrum of C_6H_5O and C_6D_5O in the A $^2B_2$ state using the scaled DFT/B3LYP/cc-pVTZ harmonic frequencies given in Tables 4 and 5. Using the error estimates from Table 6, we assume that a standard deviation from experiment of the calculated frequencies is approximately 27 cm^{-1} for C_6H_5O and 23 cm^{-1} for C_6D_5O and the maximal absolute error for the calculated frequencies is not larger than 61 cm^{-1} for C_6H_5O and 62 cm^{-1} for C_6D_5O.

Most of the calculated frequencies for the A $^2B_2$ state have very similar values to the corresponding values obtained for the ground state. Although the frequency shift for some of the vibrational modes can be large, the overall change of zero-point energy (ZPE) is only −25 cm^{-1} for C_6H_5O and −40 cm^{-1} for

TABLE 6: Comparison of Accuracy of Scaled Harmonic Frequencies Calculated Using Various Computational Approaches for the Ground State of Phenol and Phenoxyl Radical[a]

	CASSCF				DFT/B3LYP							
	cc-pVDZ		aug-cc-pVDZ		cc-pVDZ		aug-cc-pVDZ		cc-pVTZ		aug-cc-pVTZ	
	σ_{st}	σ_{max}	σ_{st}	σ_{max}	σ_{st}	σ_{max}	σ_{st}	σ_{max}	σ_{st}	σ_{max}	σ_{st}	σ_{max}
C_6H_5OH	44	152	56	183	22	45	26	46	20	42	20	44
C_6D_5OD	38	139	48	164	16	35	19	45	13	43	14	42
C_6H_5O	46	117	51	136	31	60	34	63	27	61	28	61
C_6D_5O	41	119	47	142	24	62	26	64	23	62	24	65

[a] Standard deviation σ_{st} and maximal absolute deviation σ_{max} have been calculated using all known experimental fundamental frequencies (33 for C_6H_5OH and C_6D_5OD, 26 for C_6H_5O, and 25 for C_6D_5O). All values are given in cm^{-1}.

C_6D_5O. Frequencies for 9 vibrational modes of C_6H_5O and 11 vibrational modes of C_6D_5O differ by more than 30 cm^{-1} from the corresponding frequencies of the ground state. Not surprisingly, the largest change in harmonic frequencies is observed for the vibrations involving the CO bond. For C_6H_5O, mode ν_6, corresponding to the CO stretch, is red-shifted by 167 cm^{-1}, mode ν_{30}, corresponding to the in-plane CO bending, is red-shifted by 73 cm^{-1}, and mode ν_{20}, corresponding to the out-of-plane CO bending, is blue-shifted by 38 cm^{-1} as X $^2B_1 \rightarrow$ A $^2B_2$. For C_6D_5O, the corresponding values are 217, 65, and 37 cm^{-1}, respectively. Comparison of vibrational vectors shows that most modes may change substantially upon the A $^2B_2 \leftarrow$ X $^2B_1$ excitation. For C_6H_5O, we have found that only four pairs of modes (ν_5 and ν_6, ν_9 and ν_{10}, ν_{17} and ν_{18}, and ν_{23} and ν_{24}) have mixing angle larger than 20°. Here, we assume that the vibrational modes ν_i and ν_j of the ground state span approximately the same two-dimensional vector space like the vibrational modes $\nu_i{}'$ and $\nu_j{}'$ of the excited state. The mixing angle is defined then as the angle between the vectors ν_i and $\nu_i{}'$ in this two-dimensional space. For C_6D_5O, the mixing may involve more than two modes and the situation is more complicated. For example, the vibrational mode ν_6 of A $^2B_2$, which is dominated by the CO stretch, is a mixture of ν_5, ν_6, and ν_4 of X $^2B_1$ with the mixing angle between ν_5 and $\nu_6{}'$ as large as 46°. The main reason of vibrational mode mixing is large structural change of the aromatic ring and elongation of the carbon−oxygen bond. Such a mixing is not necessarily accompanied by a large change in harmonic frequencies. For example, the mixing of ν_{23} and ν_{24} upon the A $^2B_2 \leftarrow$ X $^2B_1$ excitation affects ν_{23} by only −21 cm^{-1} and ν_{24} by only +34 cm^{-1}.

Conclusion

Accurate quantum chemical methods (CASPT2, DFT, TD-DFT) are employed to study the equilibrium geometry, excitation energies, and harmonic vibrational frequencies for the first excited electronic state (A $^2B_2$) of the phenoxyl radical. The calculated properties are compared to analogous data for the ground state. The presented results show that both the ground-state and the first excited-state wave functions are strongly dominated by single electronic configurations. The A $^2B_2 \leftarrow$ X $^2B_1$ excitation can be described as a transfer of a single electron from the lone pair of oxygen to the nonbonding $\pi_{b_1}^o$ orbital delocalized over the oxygen atom and the aromatic ring. These findings show that the usual classification of the A $^2B_2 \leftarrow$ X $^2B_1$ excitation as the n−π^* transition is not correct. The more appropriate assignment should read n−π^o or even n−π, if one takes into account the substantial stabilization of the resultant doubly occupied π_{b_1} orbital. The calculated vertical (DFT, TDDFT) and adiabatic (CASPT2) excitation energies for the A $^2B_2 \leftarrow$ X $^2B_1$ transition correspond well to experimentally determined excitation energies. Unfortunately,

this situation does not permit an unambiguous classification of the experimental findings as vertical or adiabatic excitation energies. The A $^2B_2 \leftarrow$ X $^2B_1$ excitation causes substantial geometry changes in the chinoid-like structure of C_6H_5O in the ground state. The molecular structure of the A $^2B_2$ state can be described as aromatic with an oxygen atom attached to it by a single bond. The change of the CO bond order, from approximately double in X $^2B_1$ to approximately single in A $^2B_2$, introduces also a large change in harmonic frequencies for the vibrational modes involving the CO bond. The largest change is observed for the CO stretch (−167 cm^{-1} for C_6H_5O and −217 cm^{-1} for C_6D_5O). The change of ZPE upon the A $^2B_2 \leftarrow$ X $^2B_1$ excitation is much smaller (−25 cm^{-1} for C_6H_5O and −40 cm^{-1} for C_6D_5O). The presented data show that the A $^2B_2 \leftarrow$ X $^2B_1$ excitation in C_6H_5O has quite different characteristic than the analogous transition observed[46,47] recently in the phenylthiyl radical (C_6H_5S).

Supporting Information Available: A compilation of previous theoretical equilibrium structures for the ground state of phenoxyl radical, a set of harmonic vibrational frequencies for the ground states of C_6H_5O and C_6D_5O, four sets of harmonic vibrational frequencies for phenol that have been used to determine scaling factors, and CASSCF vertical excitation energies for the low-lying states of the phenoxyl radical constitute the Supporting Information for this study. This material is available free of charge via the Internet at http://pubs.acs.org.

References and Notes

(1) Porter, G.; Wright, F. J. *Trans. Faraday Soc*. **1955**, *51*, 1469.

(2) Land, E. J.; Porter, G.; Strachan, E. *Trans. Faraday Soc.* **1961**, *57*, 1885.

(3) Hinchliffe, A.; Stainbank, R. E.; Ali, M. A. *Theor. Chim. Acta* **1966**, *95*, 5.

(4) Tripathi, G. N. R.; Schuler, R. H. *J. Chem. Phys.* **1984**, *81*, 113.

(5) Chipman, D. M.; Liu, R.; Zhou, X.; Pulay, P. *J. Chem. Phys.* **1994**, *100*, 5023.

(6) Spanget-Larsen, J.; Gil, M.; Gorski, A.; Blake, D. M.; Waluk, J.; Radziszewski, J. G. *J. Am. Chem. Soc.* **2001**, *123*, 11253.

(7) Radziszewski, J. G.; Gil, M.; Gorski, A.; Spanget-Larsen, J.; Waluk, J.; Mróz, B. J. *J. Chem. Phys.* **2001**, *115*, 9733.

(8) Platz, J.; Nielsen, O. J.; Wallington, T. J.; Ball, J. C.; Hurley, M. D.; Straccia, A. M.; Schneider, W. F.; Sehested, J. *J. Phys. Chem. A* **1998**, *102*, 7964.

Molecular Properties of the Phenoxyl Radical

J. Phys. Chem. A, Vol. 112, No. 12, 2008 **2657**

(9) Winterbourn, C. C.; Kettle, A. J. *Biochem. Biophys. Res. Commun.* **2003**, *305*, 729.

(10) Dixon, W. T.; Murphy, D. *J. Chem. Soc. Faraday Trans. 2* **1976**, *72*, 1221.

(11) Takahashi, J.; Momose, T.; Shida, T. *Bull. Chem. Soc. Jpn.* **1994**, *67*, 964.

(12) Qin, Y.; Wheeler, R. A. *J. Chem. Phys.* **1995**, *102*, 1689.

(13) Nwobi, O.; Higgins, J.; Zhou, X.; Liu, R. *Chem. Phys. Lett.* **1997**, *272*, 155.

(14) Liu, R.; Morokuma, K.; Mebel, A. M.; Lin, M. C. *J. Phys. Chem.* **1996**, *100*, 9314.

(15) Jacox, M. E. *J. Phys. Chem. Ref. Data* **2003**, *32*, 1.

(16) Mukherjee, A.; McGlashen, M. L.; Spiro, T. G. *J. Phys. Chem.* **1995**, *99*, 4912.

(17) Tripathi, G. N. R.; Schuler, R. H. *J. Phys. Chem.* **1988**, *92*, 5129.

(18) Johnson, C. R.; Ludwig, M.; Asher, S. A. *J. Am. Chem. Soc.* **1986**, *108*, 905.

(19) Gunion, R. F.; Gilles, M. K.; Polak, M. L.; Lineberger, W. C. *Int. J. Mass Spectrom. Ion Processes* **1992**, *117*, 601.

(20) Qin, Y.; Wheeler, R. A. *J. Am. Chem. Soc.* **1995**, *117*, 6083.

(21) Johnston, L. J.; Mathivanan, N.; Negri, F.; Siebrand, W.; Zerbetto, F. *Can. J. Chem.* **1993**, *71*, 1655.

(22) Radziszewski, J. G.; Gil, M.; Gorski, A.; Spanget-Larsen, J.; Waluk, J.; Mróz, B. J. *J. Chem. Phys.* **2002**, *116*, 5912.

(23) Hirata, S.; Head-Gordon, M. *Chem. Phys. Lett.* **1999**, *302*, 375.

(24) Adamo, C.; Barone, V. *Chem. Phys. Lett.* **1999**, *314*, 152.

(25) Rinkevicius, Z.; Tunell, I.; Saùek, P.; Vahtras, O.; Ågren, H. *J. Chem. Phys.* **2003**, *119*, 34.

(26) Dierksen, M.; Grimme, S. *J. Chem. Phys.* **2004**, *120*, 3544.

(27) Berden, G.; Peeters, R.; Meijer, G. *Int. Rev. Phys. Chem.* **2000**, *19*, 565.

(28) Chung, C.-Y.; Cheng, C.-W.; Lee, Y.-P.; Liao, H.-Y.; Sharp, E. N.; Rupper, P.; Miller, T. A. *J. Chem. Phys.* **2007**, *127*, 044311.

(29) Werner, H.-J. *Mol. Phys.* **1996**, *89*, 645.

(30) Celani, P.; Werner, H.-J. *J. Chem. Phys.* **2000**, *112*, 5546.

(31) Dunning, T. H., Jr. *J. Chem. Phys.* **1989**, *90*, 1007.

(32) Kendall, R. A.; Dunning, T. H., Jr.; Harrison, R. J. *J. Chem. Phys.* **1992**, *96*, 6796.

(33) Werner, H.-J.; Knowles, P. J.; Amos, R. D.; *et al.*, MOLPRO, a package of ab initio programs, version 2006.1.

(34) Frisch, M. J.; Trucks, G. W.; Schlegel, H. B.; *et al. Gaussian 03*, revision A.1; Gaussian Inc.: Pittsburgh, PA, 2003.

(35) Levy, M.; Nagy, Á. *Phys. Rev. Lett.* **1999**, *83*, 4361.

(36) Gunnarsson, O.; Lundqvist, B. I. *Phys. Rev. B* **1976**, *13*, 4274.

(37) von Barth, U. *Phys. Rev. A* **1979**, *20*, 1693.

(38) Becke, A. D. *J. Chem. Phys.* **1993**, *98*, 5648.

(39) Lee, C.; Yang, W.; Parr, R. G. *Phys. Rev. B* **1988**, *37*, 785.

(40) Kohn, W.; Sham, L. J. *Phys. Rev.* **1965**, *140*, A1133.

(41) NIST Computational Chemistry Comparison and Benchmark Database, NIST Standard Reference Database Number 101, Release 12, Aug 2005, Editor: Russell D. Johnson III, http://srdata.nist.gov/cccbdb.

(42) Hagen, K.; Hedberg, K. *J. Chem. Phys.* **1973**, *59*, 158.

(43) Caminati, W.; Melandri, S.; Favero, L. B. *J. Chem. Phys.* **1994**, *100*, 8569.

(44) Data for phenol and aniline in: Hellwege, K. H., Hellwege, A. M., Eds. *Structure Data of Free Polyatomic Molecules*; Landolt-Bornstein: Group II: Atomic and Molecular Physics, Vol. 7; Springer-Verlag: Berlin, 1976.

(45) Ratzer, C.; Küpper, J.; Spangenberg, D.; Schmitt, M. *Chem. Phys.* **2002**, *283*, 153.

(46) Lim, J. S.; Lim, I. S.; Lee, K. S.; Ahn, D. S.; Lee, Y. S.; Kim, S. K. *Angew. Chem. Int. Ed.* **2006**, *45*, 6290.

(47) Lim, I. S.; Lim, J. S.; Lee, Y. S.; Kim, S. K. *J. Chem. Phys.* **2007**, *126*, 034306.

(48) Koch, W.; Holthausen, M. C. *A Chemist's Guide to Density Functional Theory*; Wiley-VCH: Weinheim, Germany, 2000.

(49) Serrano-Andrés, L.; Pou-Amérigo, R.; Fülscher, M. P.; Borin, A. C. *J. Chem. Phys.* **2002**, *117*, 1649.

(50) Finley, J. P.; Witek, H. A. *J. Chem. Phys.* **2000**, *112*, 3958.

(51) Pou-Amérigo, R.; Merchán, M.; Ortí, E. *J. Chem. Phys.* **1999**, *110*, 9536.

(52) Evans, J. C. *Spectrochim. Acta* **1960**, *16*, 1382.

(53) Keresztury, G.; Billes, F.; Kubinyi, M.; Sundius, T. *J. Phys. Chem. A* **1998**, *102*, 1371.